JGR Planets

RESEARCH ARTICLE

10.1029/2024JE008678

Thermophysical States of $MgSiO_3$ Liquid up to Terapascal Pressures: Implications for Magma Oceans in Super-Earths and Sub-Neptunes

Haiyang Luo[1] and **Jie Deng**[1]

[1]Department of Geosciences, Princeton University, Princeton, NJ, USA

Key Points:

- Structure, the Grüneisen parameter, and viscosity of $MgSiO_3$ liquid are calculated across a wide pressure and temperature range
- Temperature and pressure dependence of the Grüneisen parameter and the underlying mechanism are revealed
- The adiabat, viscosity profile, and mass-radius relation of magma ocean exoplanets are determined

Supporting Information:

Supporting Information may be found in the online version of this article.

Correspondence to:

H. Luo and J. Deng,
haiyang.luo@princeton.edu;
jie.deng@princeton.edu

Citation:

Luo, H., & Deng, J. (2025). Thermophysical states of $MgSiO_3$ liquid up to terapascal pressures: Implications for magma oceans in super-Earths and sub-Neptunes. *Journal of Geophysical Research: Planets*, *130*, e2024JE008678. https://doi.org/10.1029/2024JE008678

Received 13 AUG 2024
Accepted 1 APR 2025

Author Contributions:

Conceptualization: Haiyang Luo, Jie Deng
Data curation: Haiyang Luo
Formal analysis: Haiyang Luo
Funding acquisition: Jie Deng
Investigation: Haiyang Luo
Methodology: Haiyang Luo, Jie Deng
Project administration: Jie Deng
Resources: Jie Deng
Software: Haiyang Luo
Supervision: Jie Deng
Validation: Haiyang Luo
Visualization: Haiyang Luo
Writing – original draft: Haiyang Luo
Writing – review & editing: Haiyang Luo, Jie Deng

Abstract Thermophysical properties of silicate liquids under extreme conditions are critical for understanding the accretion and evolution of super-Earths and sub-Neptunes. The thermal equation of state and viscosity of silicate liquids determine the adiabatic profiles and dynamics of magma oceans. However, these properties are challenging to constrain at elevated pressures in experiments. Here, we perform ab initio molecular dynamics simulations of $MgSiO_3$ liquid across a wide range of pressures (0–1,200 GPa) and temperatures (2200–14000 K) and analyze its structure, the Grüneisen parameter, and viscosity. Our results reveal clear temperature and pressure dependence of the Grüneisen parameter, which vary synchronously with the with O-O coordination number. The Grüneisen parameter shifts from positive to negative temperature dependence between ∼20 and 70 GPa, corresponding to a peak in the O-O coordination number and SiO_5 abundance. Initially, the Grüneisen parameter increases with pressure and then decreases, showing limited temperature dependence above ∼300 GPa, where its behavior resembles that of solid. Furthermore, we determine the adiabat and viscosity profiles of magma oceans in super-Earths and sub-Neptunes. The results suggest that the mantles of super-Earths and sub-Neptunes may solidify either from the bottom up or at pressures of ∼120–150 GPa, depending on the curvature of the mantle melting line. Low viscosities in magma oceans are likely to enhance convective currents and facilitate efficient differentiation. These thermophysical properties, now quantified up to terapascal pressures, enable updates to the mass-radius relation of magma ocean exoplanets, showing notable differences compared to their solid counterparts.

Plain Language Summary Large exoplanets such as super-Earths and sub-Neptunes likely experienced extreme conditions during their formation, leading to the creation of vast magma oceans. Understanding the physical properties of silicate liquids under such high pressures and temperatures is crucial for studying the formation and evolution of these exoplanets. However, it is challenging to investigate these properties in a laboratory setting due to the extreme conditions involved. Alternatively, we used advanced computer simulations to study how $MgSiO_3$ liquid, a prototypical material of magma oceans, behaves under pressures up to 1,200 GPa and temperatures up to 14000 K. We found that $MgSiO_3$ liquid densifies upon compression with an increasingly small interatomic distance and generally more neighboring atoms. We determined a key property called the Grüneisen parameter, which governs the cooling and solidification processes of magma oceans. The results suggest that the mantles of super-Earths and sub-Neptunes might solidify from the bottom up or from the middle out. We also studied the viscosity and mass-radius relation of exoplanets which are fully molten. The low viscosity suggests strong convective currents, leading to efficient mixing and differentiation of materials within these exoplanets. The updated mass-radius relation can be used to more accurately constrain the thermophysical state of exoplanets.

1. Introduction

During planetary accretion, giant impacts and radioactive decay likely extensively melt planets (Canup, 2004; Elkins-Tanton, 2012). Super-Earths and sub-Neptunes, with approximately 1–10 times the mass of Earth, are among the two groups of commonly found exoplanets (Charbonneau et al., 2009; Fortney et al., 2007; Fulton et al., 2017; Valencia et al., 2007). Both planet groups may be largely molten by the end of energetic accretion, forming deep magma oceans (Boujibar et al., 2020; Fei et al., 2021; Stixrude, 2014). These magma oceans are believed to be long-lived (Vazan et al., 2018), possibly still active today, due to their high initial temperatures and limited cooling resulting from intense irradiation from their host stars and potentially thick atmospheres.

Knowledge of the structure, thermodynamics, and viscosity of silicate liquids under the pressure (up to ~1,400 GPa) and temperature (up to ~14000 K) conditions of super-Earths' and sub-Neptunes' mantles is essential for understanding the accretion, evolution, and dynamics of these exoplanets. For example, the Grüneisen parameter controls the adiabatic thermal profiles of magma oceans (Stixrude et al., 2009). The mantle melting line and the adiabat together determine the solidification mode of the mantle, including bottom-up, middle-out, and top-down. The viscosity governs the dynamics of magma oceans and affects petrologic and geodynamic processes, including crystal settling and core-mantle differentiation (Karki & Stixrude, 2010; Luo et al., 2021; Solomatov, 2007). These properties of silicate liquids have been well documented under Earth-relevant conditions (Bajgain et al., 2022; Caracas, 2024; Caracas et al., 2019; Caracas & Stewart, 2023; de Koker & Stixrude, 2009; Karki & Stixrude, 2010; Luo et al., 2021; Solomatova & Caracas, 2019; Stixrude & Karki, 2005) and yet remain largely unconstrained under conditions beyond the Earth (Morard et al., 2024). Direct experimental measurement of these properties at these extreme conditions is challenging. Shock-wave experiments have been performed to study the Grüneisen parameter of silicate liquids under extreme compression (Fratanduono et al., 2018; Mosenfelder et al., 2009), but the values are subject to large uncertainties, and the temperature dependence of the Grüneisen parameter is difficult to constrain.

Several ab initio studies have investigated the properties of silicate liquids under the conditions of super-Earths and sub-Neptunes (Bardon, 2018; Militzer, 2013; Soubiran & Militzer, 2018; Zhao et al., 2014), but their data are relatively sparse and mainly focused on heat capacity, electrical conductivity, and liquid-liquid transition. Another ab initio study examined warm dense silicate under even more extreme conditions (10^4–10^8 K) (González-Cataldo et al., 2020). The pressure and temperature dependence of the Grüneisen parameter under the conditions of super-Earths' and sub-Neptunes' interiors were not resolved. The thermal and viscosity profiles of magma oceans in super-Earths and sub-Neptunes were not well constrained either.

Here, we systematically study the structure, thermodynamics, and viscosity of $MgSiO_3$ liquid, a prototypical material of magma oceans in rocky planets, across a wide range of pressures (0–1,200 GPa) and temperatures (2200–14000 K) by performing extensive ab initio molecular dynamics simulations. These simulations provide insights into the thermophysical properties of $MgSiO_3$ liquid at extreme conditions, enabling the establishment of adiabatic thermal profiles and viscosity profiles for magma oceans in super-Earths and sub-Neptunes.

2. Materials and Methods

2.1. Molecular Dynamics Simulations

We performed Born-Oppenheimer ab initio molecular dynamics (AIMD) simulations of $MgSiO_3$ liquid using 160 atoms (32 formula units of $MgSiO_3$), covering a volume range 3.6–15.6 $Å^3$/atom (3.6, 3.9, 4.2, 4.8, 5.4, 6.0, 6.6, 8.4, 9.6, 10.8, 12.0, 13.2, and 15.6 $Å^3$/atom) and a temperature range 2200–14000 K (2200, 3000, 5000, 8000, 10000, 12000, and 14000 K). We conducted simulations using 320 atoms (64 formula units of $MgSiO_3$) for the smallest system with a volume of 3.6 $Å^3$/atom and found that the size effect on the structure of $MgSiO_3$ liquid is negligible (Figure S1 in Supporting Information S1). The size effect on the viscosity was also shown to be insignificant (Luo et al., 2021). All the simulations were performed using projector augmented wave (PAW) method (Blochl, 1994; Kresse & Joubert, 1999) as implemented in the Vienna Ab-initio Simulation Package (VASP) (Kresse & Furthmüller, 1996). We used the PBEsol exchange-correlation functional (Perdew et al., 2008) as it has previously shown good agreement with experimental measurements of physical properties of silicates (Deng & Stixrude, 2021; Holmström & Stixrude, 2015; Scipioni et al., 2017). The PAW potentials utilized had the following valence configurations: Mg $2p^6 3s^2$, Si $3s^2 3p^2$, and O $2s^2 2p^4$ with core radii of 1.058, 1.005, and 0.804 Å, respectively. These PAW potentials have been widely used and proven to be robust up to at least 1,000 GPa (Fei et al., 2021; Root et al., 2018; Soubiran & Militzer, 2018). We assumed thermal equilibrium between ions and electrons using the Mermin functional (Mermin, 1965), explicitly considering the effect of finite electronic temperature. We reported the projected densities of states under different pressures at 14000 K as an example in Figure S2 in Supporting Information S1. Gamma Point Brillouin zone sampling with an energy cutoff of 800 eV was applied, which was sufficient to converge the pressure within 0.16 GPa and the energy within 1 meV per atom. We used a canonical ensemble (NVT) with temperature controlled by a Nosé-Hoover thermostat (Nose, 1984). Each simulation was run for up to ~10,000–20,000 steps with a timestep of 1.0 femtosecond (fs). Simulations under high pressures/low temperatures were performed for a longer period than those under low pressures/high temperatures. The values and errors of pressure and energy were estimated using the block

averaging method (Flyvbjerg & Petersen, 1989). We monitored radial distribution functions (RDF) and mean-square displacements (MSD) to ensure the liquid/fluid state of our simulated systems. Examples of calculated MSD at 10,000 K and 12,000 K at the smallest volume (3.6 Å^3/atom) explored are shown in Figure S3 in Supporting Information S1.

The coordination number (n) of type A with respect to type B can be expressed through the RDF $g_{\mathrm{AB}}(r)$:

$$n_{\mathrm{AB}} = 4\pi\rho_B \int_0^{r_{\mathrm{min}}^{\mathrm{AB}}} r^2 g_{\mathrm{AB}}(r)\mathrm{d}r, \tag{1}$$

where ρ is the density and $r_{\mathrm{min}}^{\mathrm{AB}}$ is the position of the first minimum in $g_{\mathrm{AB}}(r)$. The bond length is reported as the average distance within $r_{\mathrm{min}}^{\mathrm{AB}}$. Detailed structural analysis was conducted using the UMD package (Caracas et al., 2021).

The viscosity was calculated using the Green-Kubo relation

$$\eta = \frac{V}{3k_{\mathrm{B}}T}\sum_{i,j}\int_0^{\infty} \langle \tau_{ij}(t+t_0)\cdot\tau_{ij}(t_0)\rangle\, dt, \tag{2}$$

where V is volume, k_B is the Boltzmann constant, T is the temperature, τ_{ij} is the ij off-diagonal component of the stress tensor, t is time, and $\langle\cdots\rangle$ is an average over time origins t_0.

2.2. Equation of State

To describe the thermodynamic property of $MgSiO_3$ liquid across a wide P-V-E-T space and to self-consistently capture the nonmonotonic change of the Grüneisen parameter with compression, we adopted the equation of state (EOS) recently developed by Wolf & Bower, 2018. This EOS, named the RTpress EOS, comprises an isothermal part and a thermal perturbation given by a generalized Rosenfeld-Tarazona (RT) model. Other commonly used EOSs are either not thermodynamically self-consistent in the P-V-E-T space or fail to describe the nonmonotonic nature of the Grüneisen parameter of $MgSiO_3$ melt. For example, previously used thermal equations of state, such as the modified Holland-Powell equation (Angel et al., 2014; Holland & Powell, 1998) and the simplified Mie-Grüneisen equation (Karki, 2010), are self-consistent in the P-V-T space but omit energy (E) terms. This omission affects the accuracy of the derived thermodynamic properties that depend on both P-V-T parameters and energy, such as heat capacity and the Grüneisen parameter. Other Mie-Grüneisen forms may self-consistently include energy terms but yield a monotonic variation of the Grüneisen parameter with volume (de Koker & Stixrude, 2009).

The RTpress EOS can be expressed as

$$P(V,T) = P(V,T_0) + \Delta P_E(V,T) + \Delta P_s(V,T), \tag{3}$$

where $P(V,T_0)$ is the isothermal component describe by the Vinet EOS:

$$P(V,T_0) = 3K_0\left(\frac{V}{V_0}\right)^{-2/3}\left[1-\left(\frac{V}{V_0}\right)^{1/3}\right]\exp\left[\frac{3}{2}\left(K_0'-1\right)\left(1-\left(\frac{V}{V_0}\right)^{1/3}\right)\right], \tag{4}$$

where model parameters V_0, K_0, and K_0' are the volume, isothermal bulk modulus, and derivative of isothermal bulk modulus at the reference temperature T_0 and zero pressure. $\Delta P_E(V,T)$ and $\Delta P_s(V,T)$ are the energetic and entropic contributions to the thermal perturbation, respectively, and can be written as

$$\Delta P_E(V,T) = -b'(V)\left[f_T(T) - f_T(T_0)\right], \tag{5}$$

$$\Delta P_S(V,T) = \frac{b'(V)}{m-1}\left[T\left(f_T'(T) - f_T'(T_{0S})\right) - T_0\left(f_T'(T) - f_T'(T_{0S})\right)\right] + \gamma_{0S}(V)\,\frac{C_{V,0S}(V)\,(T-T_0)}{V}, \tag{6}$$

where the thermal coefficients $b'(V) = \sum_n b_n (V/V_0 - 1)^n$ and the thermal deviation from the reference temperature $f_T = (T/T_0)^m - 1$, in which $m = 0.6$. T_{0S}, $\gamma_{0S}(V)$, and $C_{V,0S}(V)$ are the temperature, the Grüneisen parameter, and heat capacity along the reference adiabat. Specifically, in the RTpress EOS, the Grüneisen parameter can be expressed as

$$\gamma = \gamma_{0S}(V)\frac{C_{V,0S}}{C_V(V,T)} + V\frac{b'(V)}{b(V)}\frac{(S^{\text{pot}}(T) - S^{\text{pot}}(T_{0S}))}{C_V(V,T)}. \quad (7)$$

More details of the RTpress EOS can be found in Wolf and Bower (2018).

3. Results and Discussion

3.1. The RTpress Equation of State

Figure 1 displays our pressure, volume, temperature, and energy data along with the best-fit RTpress EOS model. As shown, the model accurately reproduces the AIMD data, with average residual uncertainties of 3 GPa in pressure and 0.06 eV/atom in energy, which are comparable to those based on classical MD simulation data and are much smaller than those using AIMD data at Earth's conditions (Wolf & Bower, 2018). Considering that the ranges of pressure and energy variations here are about 10 times larger than in previous molecular dynamics (MD) simulations (de Koker & Stixrude, 2009; Spera et al., 2011), the uncertainties we obtain are reasonable. Table 1 summarizes the EOS parameters and their uncertainties compared to the parameters based on the two MD simulation data sets at Earth's mantle conditions. The volume per atom (V_0), the isothermal bulk modulus (K_0), and the bulk modulus pressure derivative (K_0') we obtained at 3000 K are 14.352 ± 0.048 Å^3, 13.53 ± 0.35 GPa, and 6.767 ± 0.040 GPa, respectively. These values agree quite well with previous studies (de Koker & Stixrude, 2009; Spera et al., 2011) from which the derived ranges of V_0, K_0, and K_0' are 12.93–14.85 Å^3, 9.05–13.39 GPa, and 7.27–8.29 GPa, respectively, especially considering that we employed the PBEsol exchange-correlation functional, differing from previous works. Furthermore, as shown later in Figures 6 and 7, our calculated Grüneisen parameter and viscosity are consistent with previous studies (de Koker & Stixrude, 2009; Luo et al., 2021) within the common pressure and temperature ranges explored.

3.2. $MgSiO_3$ Liquid Structure

Increasing pressure leads to more tightly packed structures of $MgSiO_3$ liquid with decreasing bond lengths and increasing coordination numbers. An example at 10000 K is shown in Figure 2. Figure 3 shows the detailed changes of Si-O, Mg-O, O-O, and Si-Si bond lengths and the corresponding coordination numbers. O and O (as well as Si and Si) do not form conventionally defined bonds, and the interatomic distances and their coordination numbers reflect the overall change of $MgSiO_3$ liquid structure. From zero pressure to 1,161 GPa, Mg-O, O-O, and Si-Si bond lengths decrease monotonically from ∼2.25 to 1.66 Å, ∼3.00 to 1.93 Å, and ∼3.12 to 2.50 Å, respectively. In comparison, the Si-O bond length initially increases from ∼1.68 to 1.76 Å until ∼50 GPa at relatively low temperatures (<∼5000 K) and then decreases to 1.57 Å. The notable temperature dependence of the Si-O bond length at low pressures is due to the variation in Si-O coordination species with temperature. Our calculated bond lengths for Mg-O, O-O, and Si-O are consistent with earlier ab initio results under Earth's mantle conditions (<135 GPa) (Kim et al., 2019; Stixrude & Karki, 2005).

The corresponding changes in Si-O, Mg-O, O-O, and Si-Si coordination numbers are intriguing. The Si-O coordination number increases from ∼4.0 at zero pressure to 7.8 at 1,161 GPa. The Si-Si coordination number is only ∼2.3 at zero pressure, much lower than the Si-O coordination number, and it increases rapidly and behaves similarly to the Si-O coordination number above ∼50–80 GPa. The Mg-O coordination number is ∼4.8 at zero pressure and rapidly increases to ∼8.2 at 200 GPa, then grows marginally with further compression. In contrast, the O-O coordination number is ∼9.8 at zero pressure and then rises steeply to a peak value of ∼13.3 at ∼20–70 GPa. With further compression, the O-O coordination number decreased quickly and plateaued with an average value of 9.5–10.4 at >∼300–380 GPa. The peak position of the O-O coordination number corresponds very well with the highest abundance of Si-5O coordination species (SiO_5) (Figure 3), indicating that the initial increase and subsequent decrease in the O-O coordination number are primarily controlled by the SiO_5 abundance. Figure 4 shows detailed changes in the abundances of different Si-O coordination species. As compression

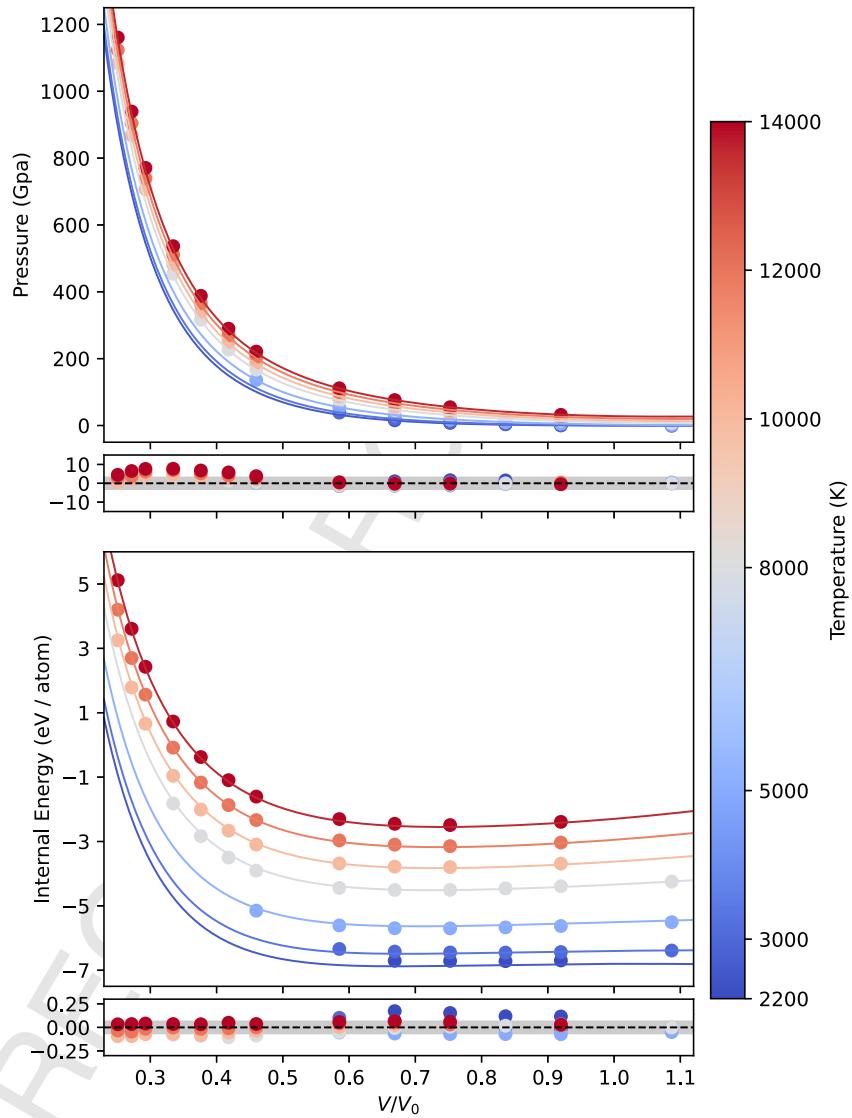

Figure 1. The RTpress equation of state for $MgSiO_3$ melt. The upper and lower panels display the isothermal compression curves (color-coded) in terms of pressure and internal energy, respectively, along with the corresponding model residuals. The average root mean square errors (RMSE), represented by the gray band, are approximately 3 GPa and 0.06 eV/atom.

increases, the abundances of SiO_5, SiO_6, and SiO_7 all initially increase to certain pressures, followed by a decrease in their abundances. In contrast, SiO_8 and SiO_9 abundances continue to increase at least up to 1,200 GPa. Similarly, Figure 5 shows detailed changes in the abundances of different O-Si coordination species. The O-Si coordination species is an extended concept of the commonly used non-bridging oxygen and bridging oxygen as O bonding with three and four Si (referred as OSi_3 and OSi_4, respectively) emerges at extreme pressures. Increasing compression results in a rapid decline in the abundance of OSi species but a growth in those of OSi_3 and OSi_4 species. In contrast, the abundance of OSi_2 species first increases reaching a peak at ~75–150 GPa depending on the temperature, and then decreases with pressure.

3.3. The Grüneisen Parameter of $MgSiO_3$ Melt

We calculated the Grüneisen parameter (γ) of $MgSiO_3$ liquid using the finite difference method, that is, $\gamma = V(\partial P/\partial E)_V$ within several temperature intervals (2200–3000 K, 3000–5000 K, 5000–8000 K, 8000–10000 K, 10000–12000 K, and 12000–14000 K, respectively). As shown in Figure 6, the Grüneisen parameter first increases with compression and then decreases, with a turning point at the volume of 5.4 $Å^3$/atom

Table 1
The RTpress Equation of State Parameters for $MgSiO_3$ Melt

Parameters	This study	dK09	S11
T_0 (K)	3,000	3,000	3,000
m	0.6	0.6	0.6
V_0 (Å^3/atom)	14.352(48)	14.74(11)	12.949(18)
K_0 (GPa)	13.53(35)	9.77(72)	13.20(19)
K_0' (GPa)	6.767(40)	7.42(15)	8.238(49)
E_0 (eV/atom)	−6.399(19)	−6.850(15)	−20.5953(19)
γ_0	0.158(15)	0.282(22)	0.1899(53)
γ_0'	−1.710(58)	−1.35(15)	−1.940(35)
b_0 (eV/atom)	1.763(25)	1.118(55)	0.9821(97)
b_1 (eV/atom)	0.982(61)	−0.05(12)	0.615(60)
b_2 (eV/atom)	2.11(16)	2.1(11)	1.31(27)
b_3 (eV/atom)	0.37(70)	12.9(60)	−3.0(17)
b_4 (eV/atom)	1.9(10)	15.5(70)	−4.1(29)

Note. Our fitted parameters are compared to previous fitting results (Wolf & Bower, 2018) based on molecular dynamics simulations under Earth's mantle conditions (de Koker & Stixrude, 2009; Spera et al., 2011). 1σ uncertainties are reported.

corresponding to ~300–380 GPa depending on the temperature. The Grüneisen parameter also exhibits a positive temperature dependence at volumes >9.6 Å^3/atom, despite an anomalous change from 12,000 to 14000 K. This temperature dependence is opposite to that observed when the volume is smaller than 8.4 Å^3/atom. The turning point of the temperature dependence of the Grüneisen parameter, which depends on the temperature itself, is located close to the range of 8.4–9.6 Å^3/atom.

We find that the two turning points associated with the temperature and volume dependence of the Grüneisen parameter correspond very well to the peak and plateau of the O-O coordination number with compression. This suggests that the O-O coordination number is a good indicator of the changes in the Grüneisen parameter with compression in $MgSiO_3$ melt, which could also apply to other silicate liquids. The peak in the O-O coordination number reflects an adjustment in the overall $MgSiO_3$ liquid structure and can be associated with the abundance change of the transitional five coordinated silicon (SiO_5), which leads to the change in the temperature dependence of the Grüneisen parameter. The plateau in O-O coordination number, combined with the slow increase in Mg-O and Si-O coordination numbers, indicates that the $MgSiO_3$ liquid in this region develops more solid-like behavior under compression. It is known that the Grüneisen parameter of solids decreases with compression and

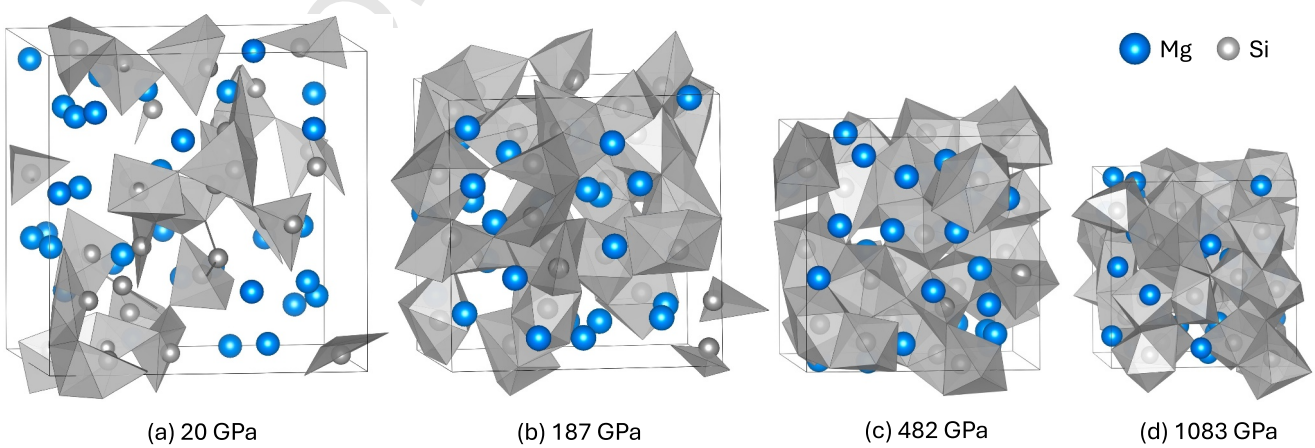

Figure 2. $MgSiO_3$ liquid structure. The four snapshots are taken from the simulations at 10,000 K under (a) 20 GPa, (b) 187 GPa, (c) 482 GPa, and (d) 1,083 GPa. SiO_x is shown as gray polyhedral. MgO_x is not shown for clarity. The average Si-O coordination number are (a) 4.0, (b) 6.2, (c) 7.1, and (d) 7.8.

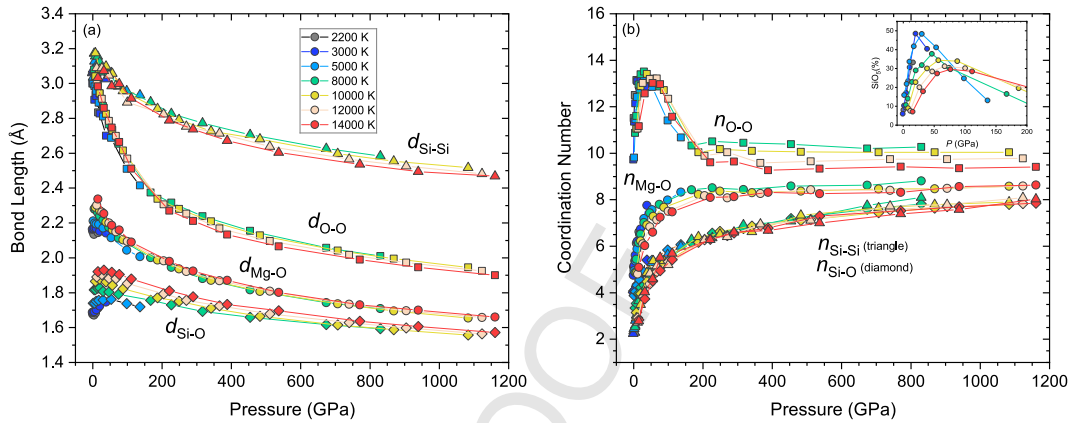

Figure 3. Structure of $MgSiO_3$ liquid as a function of pressure. Different colors represent different temperatures (2200 K-gray; 3000 K-dark blue; 5000 K-blue; 8000 K-green; 10,000 K-yellow; 12,000 K-light red; 14,000 K-red). (a) Si-O, Mg-O, O-O, and Si-Si bond lengths; (b) corresponding mean coordination numbers for Si-O, Mg-O, O-O, and Si-Si; The insert panel shows the abundances of SiO_5 as a function of pressure (<200 GPa) at different temperatures, corresponding to the change in O-O coordination number.

shows very limited temperature dependence (Boehler et al., 1979). These two features are clearly observed in $MgSiO_3$ liquid when the pressure is above ~300 GPa.

A recent shock wave experiment reported a Grüneisen parameter value of 0.92 ± 0.08 at ~300 GPa with a volume of ~5.3 $Å^3$/atom (Fratanduono et al., 2018), in good agreement with our results. A previous ab initio study under Earth's conditions (de Koker & Stixrude, 2009) also found that with compression, the Grüneisen parameter initially increases to some extent before decreasing, but a monotonic model between the Grüneisen parameter and compression was assumed. Similar monotonic increasing trends were also adopted in another study (Mosenfelder

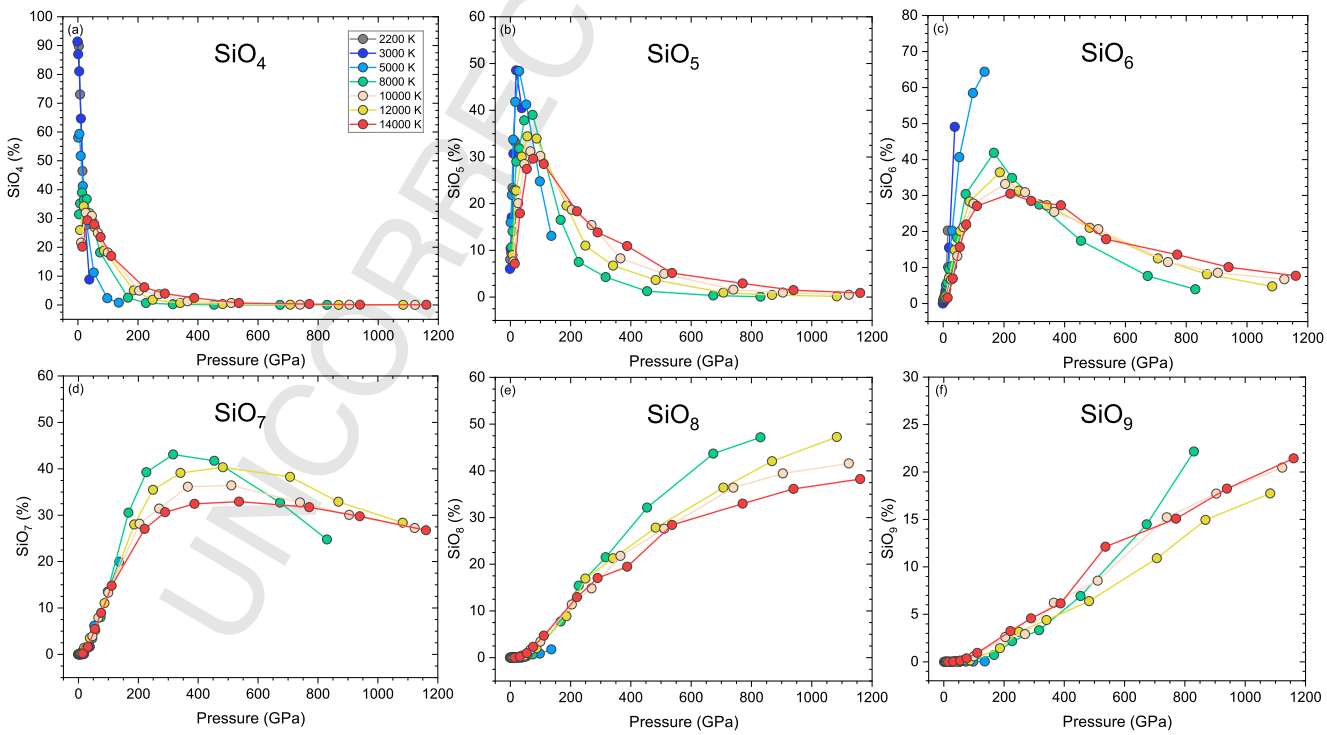

Figure 4. Abundance of Si-O coordination species. Different colors represent different temperatures (2200 K-gray; 3000 K-dark blue; 5000 K-blue; 8000 K-green; 10,000 K-yellow; 12,000 K-light red; 14,000 K-red). Different panels correspond to different Si-O coordination species, SiO_4 (a), SiO_5 (b), SiO_6 (c), SiO_7 (d), SiO_8 (e), and SiO_9 (f).

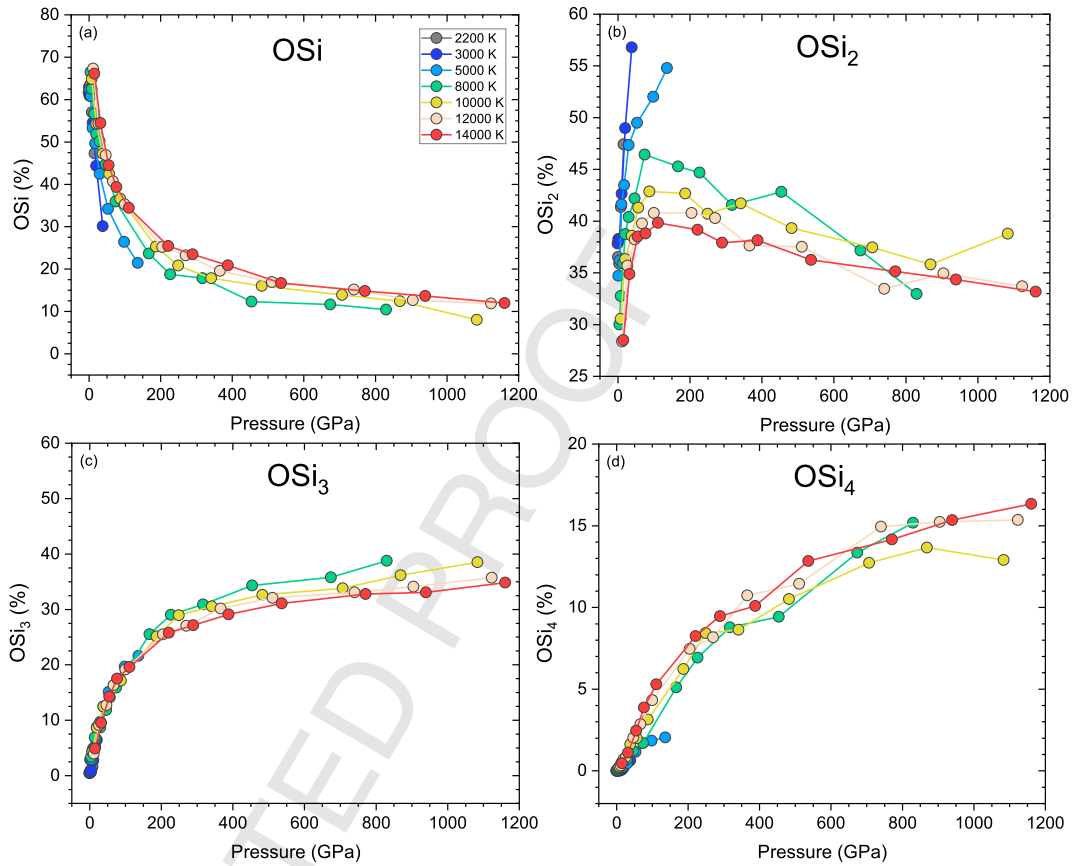

Figure 5. Abundance of O-Si coordination species. Different colors represent different temperatures (2200 K-gray; 3000 K-dark blue; 5000 K-blue; 8000 K-green; 10,000 K-yellow; 12,000 K-light red; 14,000 K-red). Different panels correspond to different O-Si coordination species: OSi (a), OSi_2 (b), OSi_3 (c), and OSi_4 (d).

et al., 2009). The values of the Grüneisen parameter we calculated are broadly consistent with previous experimental (Fratanduono et al., 2018; Mosenfelder et al., 2009) and computational studies (de Koker & Stixrude, 2009). However, as shown in Figure 6, to accurately derive adiabatic thermal profiles of super-Earths and sub-Neptunes which reach multi-megabar pressures, it is essential to capture the non-monotonic behavior of the Grüneisen parameter with respect to volume and temperature, as done here using the RTpress EOS model. It is worth noting that there are small misfits in the Grüneisen parameter at the smallest volumes for temperatures below 5000 K. While using piecewise fitting by considering multiple segments of temperature reduces the misfit, it may result in an overfitted and discontinuous model. Considering that the minor inconsistency between the fitted RTpress EOS and the simulation data under such extreme conditions does not significantly affect our results, we chose to use a universal RTpress EOS model.

3.4. Viscosity of $MgSiO_3$ Melt

The extremely high-temperature regime explored in this study (5000–14000 K) allows us to estimate viscosity up to terapascal pressures within a relatively short simulation time (<20 picoseconds) (Figure S4 in Supporting Information S1). We calculated the viscosity of $MgSiO_3$ liquid at 5000, 8000, 10000, 12000, and 14000 K, respectively. Our calculated viscosity at 5000 K aligns well with previous studies (Karki & Stixrude, 2010; Luo et al., 2021). Although the simulation time of this study is sufficient to obtain converged EOS properties, it is not long enough to converge the viscosity at relatively low temperatures (2200 and 3000 K). As such, we plotted the viscosity data at the two temperatures from prior work, which used a machine learning potential (Luo et al., 2021) as a reference. As shown in Figure 7, viscosity always increases with pressure (at $T > 3000$ K) and decreases with temperature. Due to these two competing effects, viscosity remains low at ultrahigh pressures and temperatures. For instance, at 8000 K, the viscosity increases from 0.0052 to 0.044 Pa·s within the pressure range of 167–

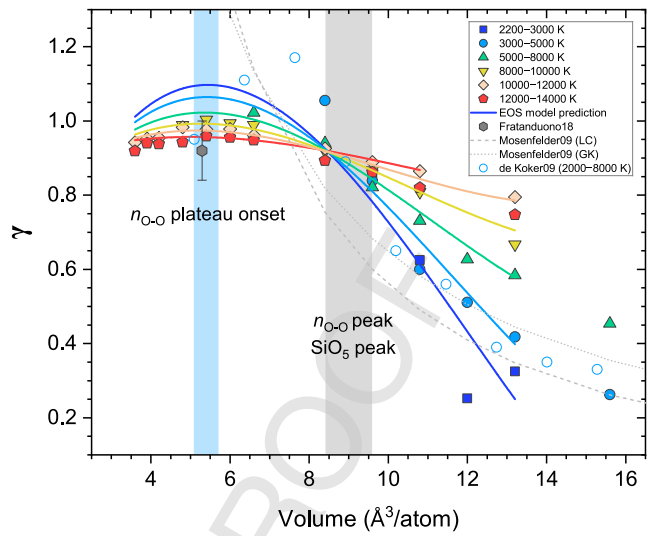

Figure 6. Volume and temperature dependence of the Grüneisen parameter in $MgSiO_3$ melt. The symbols, directly calculated from our molecular dynamics simulations using the finite difference method with the equation $\gamma = V(\partial P/\partial E)_V$, show overall good consistency with the values (lines) predicted by our fitted RTpress equation of state (EOS) at the mean temperatures of the shown intervals. The turning points of the temperature and volume dependence of the Grüneisen parameter correspond to the peak and the plateau onset of the O-O coordination number with compression, respectively. The peak of the O-O coordination number also coincides with the peak abundance of SiO_5. Estimations of the Grüneisen parameter by previous experiments, that is, gray hexagon (Fratanduono et al., 2018), dashed line (Mosenfelder et al., 2009), and dotted line (Mosenfelder et al., 2009) and calculations, open blue circles (de Koker & Stixrude, 2009) are also displayed.

674 GPa. At 12,000 K, the viscosity increases from 0.0029 to 0.027 Pa·s with increasing pressure from 204 to 1,123 GPa. Our data can be described by a piecewise modified VFT (Vogel-Fulcher-Tammann) equation (Karki & Stixrude, 2010; Luo et al., 2021): $\eta(P,T) = \exp\left[-4.544 - 0.029\,P + 0.0411\,P^2/1000 + \left(-7504 + 225\,P - 0.282\,P^2\right)/(T - 1000)\right]$ for $5000 \le T \le 8000$ K; and $\eta(P,T) = \exp\left[-8.008 + 0.00366\,P - 0.00282\,P^2/1000 + \left(15596 + 1.979\,P + 0.0196\,P^2\right)/(T - 1000)\right]$, for $8000 \le T \le 14000$ K.

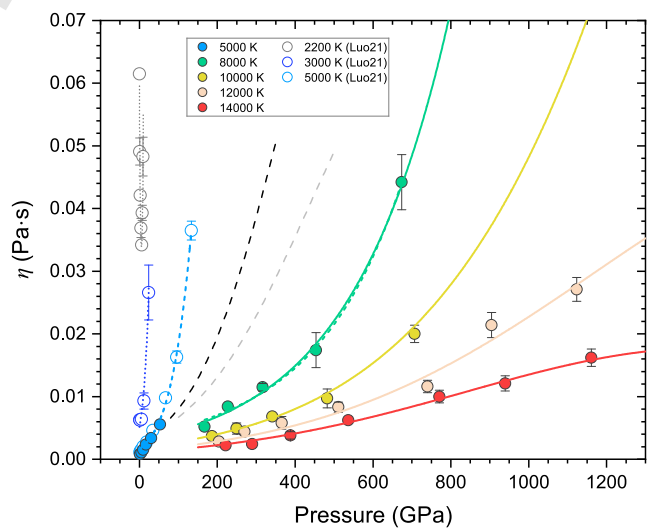

Figure 7. Viscosity of $MgSiO_3$ liquid as a function of pressure at different temperatures. Solid symbols represent our calculated results from molecular dynamics simulations. Open symbols and the corresponding dotted lines represent data and fits from a previous study (Luo et al., 2021). Solid and dashed lines represent the fitted results within two temperature ranges (5000–8000 K and 8000–14000 K), respectively, which overlap well at 8000 K. The dashed lines in dark gray and light gray show the predicted viscosity at 6500 and 7000 K, respectively.

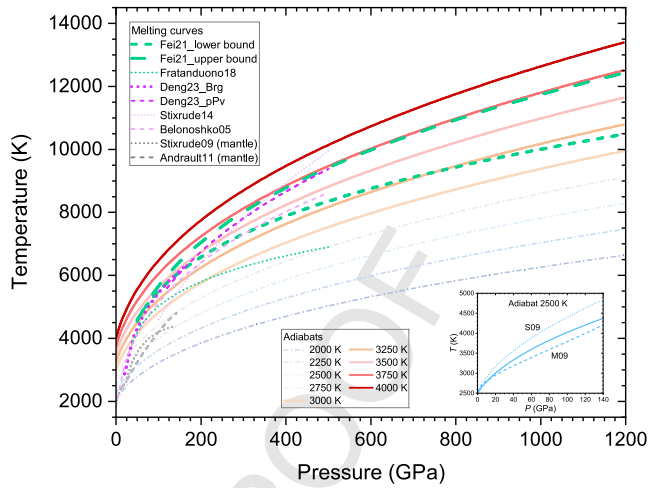

Figure 8. Adiabatic thermal profiles in a magma ocean based on $MgSiO_3$ liquid results. Solid and dash-dotted lines of different colors represent the adiabats corresponding to various potential temperatures at the surface. The dash-dotted lines with transparency below 3000 K indicate results that are likely unrealistic at high pressures where $MgSiO_3$ may remain solid. The insert panel compares our calculated 2500 K adiabat with two previously reported results (Mosenfelder et al., 2009; Stixrude et al., 2009). Green long-dashed and short-dashed lines represent the upper bound and lower bound of $MgSiO_3$ melting lines, respectively, constrained by shock compression experiments using bridgmanite under the conditions of super-Earths and sub-Neptunes (Fei et al., 2021). Green dotted line is the melting curve from laser-shock of enstatite (Fratanduono et al., 2018). Purple dotted and dashed lines are computational melting lines of bridgmanite and post-perovskite with a machine learning potential (Deng et al., 2023). Other $MgSiO_3$ melting lines reaching the regime of post-perovskite include the one inferred from the Lindemann law (Stixrude, 2014) and the result from two-phase simulations based on classical potential with corrections (Belonoshko et al., 2005). Gray dotted and dashed lines represent Earth's mantle melting curve (liquidus) (Andrault et al., 2011; Stixrude et al., 2009).

4. Implications

4.1. Adiabatic Temperature Profile of Magma Ocean

Crystallization of magma oceans profoundly influences the structure and composition of the mantles of super-Earths and sub-Neptunes (Fei et al., 2021; Stixrude, 2014). The crystallization pathway of a magma ocean—whether bottom-up, middle-out, or top-down—depends on the relative curvature of the adiabat of the magma oceans and the mantle melting curve (liquidus). If the slope of an adiabat is shallower than that of the melting line, the magma ocean will crystallize from the bottom up. In contrast, if the adiabat is tangent to the melting line at middle or shallow mantle depths defined by the conditions of super-Earths and sub-Neptunes, crystallization can initiate well above the bottom of the mantle.

We calculated the adiabats of magma oceans based on the Grüneisen parameter predicted by our RTpress EOS model for $MgSiO_3$ liquid using the equation $(dT/dP)_S = \gamma(T/K_S)$. The isentropic bulk modulus K_S was calculated by $K_S = K_T(1 + \alpha\gamma T)$, where the isothermal bulk modulus $K_T = -V(\partial P/\partial V)_T$ and α represents the thermal expansion coefficient. The calculated isentropic bulk modulus and the Grüneisen parameter along the adiabats are shown in Figure S5 in Supporting Information S1. Figure 8 presents the adiabatic temperature profiles up to 1,200 GPa across a range of temperatures, with colors representing their potential temperature at zero pressure. Magma oceans of super-Earths and sub-Neptunes may have a wide range of potential temperatures. As the mantle liquidus in super-Earths and sub-Neptunes has not been determined yet, we discuss the crystallization pathway of their mantles using the $MgSiO_3$ melting line as a first-order approximation. Only previous melting curves based on data beyond megabar pressures are considered. Several $MgSiO_3$ melting lines constrained by experiments (Fei et al., 2021; Fratanduono et al., 2018), MD simulations (Belonoshko et al., 2005; Deng et al., 2023), and the Lindemann law (Stixrude, 2014) are plotted. As shown, the threshold adiabat just before crystallization has a potential temperature of around 3750 K based on the upper bound of $MgSiO_3$ melting curve of Fei et al., 2021, and this adiabat almost overlaps with the melting line at extreme pressures, meaning that the magma ocean would begin to crystallize at or near the base of the mantle up to at least 1,200 GPa. However, the potential temperature of the threshold adiabat decreases to about 3500 K, and the crystallization would initiate

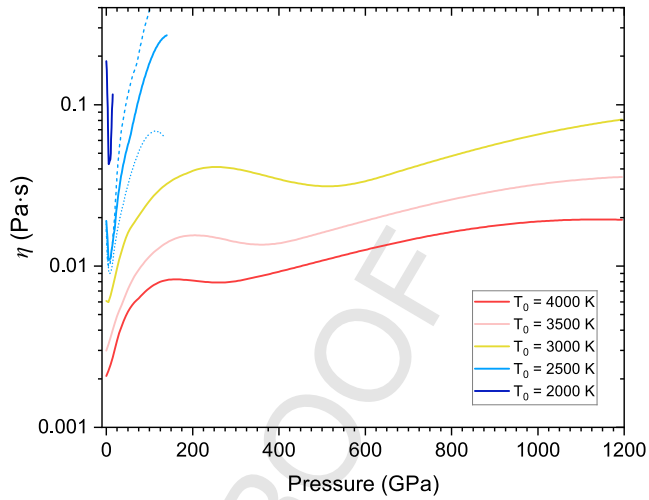

Figure 9. Viscosity profiles along adiabats in a magma ocean based on $MgSiO_3$ liquid results. Lines of different colors represent viscosity profiles corresponding to various potential temperatures (2000, 2500, 3000, 3500, and 4000 K) at zero pressure. The temperatures increase with pressure along the adiabats as shown in Figure 8. The dashed and dotted lines represent the calculated viscosity profiles using previously reported ~2500 K adiabats from Stixrude (2009) and Mosenfelder et al. (2009), respectively.

at approximately 120–150 GPa based on the lower bound of $MgSiO_3$ melting curve reported by Fei et al., 2021. Additionally, the two MD results (Belonoshko et al., 2005; Deng et al., 2023) predict threshold potential temperatures of 3750 and 3500 K, respectively, with crystallization onset at or near the base of the mantle up to at least 500 GPa. As the curvature of the mantle liquidus in super-Earths and sub-Neptunes remains an open question, the crystallization mode of the mantles is yet to be fully resolved. Nevertheless, the upper limit of the potential temperature for magma ocean crystallization is approximately 3750 K according to our results.

4.2. Viscosity Profile of Magma Ocean

Viscosity plays a critical role in regulating the dynamics and evolution of magma oceans (Solomatov, 2007). By combining our results with previous computational data (Luo et al., 2021), we evaluated the viscosity profiles of magma oceans up to 1,200 GPa along several adiabats at potential temperatures of 2000, 2500, 3000, 3500, and

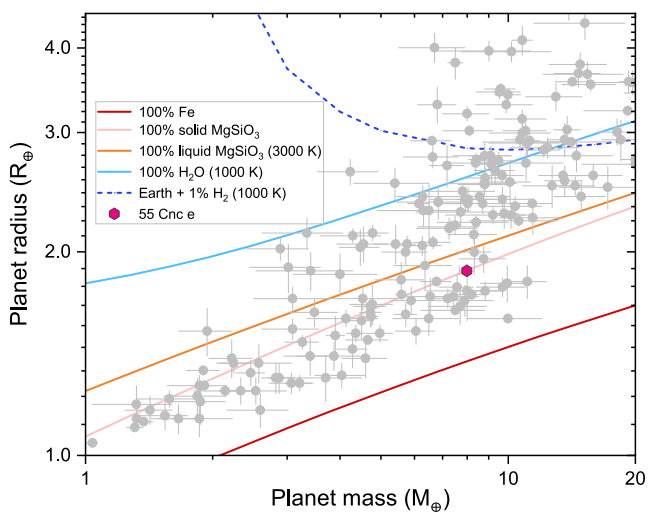

Figure 10. Mass-radius relation of exoplanets. The different lines represent mass-radius relations for planets of representative endmember compositions. The 100% liquid $MgSiO_3$ line is derived based on our calculated equation of state and the adiabat with a surface potential temperature of 3000 K as shown in Figure 8. Using a different potential temperature does not significantly alter the line. All other lines are taken from Zeng et al. (2019).

4000 K under the conditions of super-Earths and sub-Neptunes. As shown in Figure 9, the viscosity profiles along the 2000 and 2500 K adiabats are similar to (Luo et al., 2021), with a minimum at approximately 6–7 GPa, depending on the potential temperature. Along the 3000, 3500, and 4000 K adiabats, the viscosity increases about 10 times from zero pressure to 1,200 GPa, despite a shallow local maximum. For instance, the viscosity increases from 0.006 to 0.08 Pa·s along the 3000 K adiabat. Along the 4000 K adiabat, the viscosity increased from 0.002 to 0.019 Pa·s. It is likely that a certain amount of water may dissolve into the magma ocean, but its influence on viscosity at ultrahigh pressures and temperatures is limited (Karki & Stixrude, 2010). The composition of magma oceans on super-Earths and sub-Neptunes varies significantly given the vast range of composition of their host stars (Hinkel et al., 2024). Previous studies suggest that the viscosity of $MgSiO_3$ liquid is slightly higher or comparable to that of basaltic melt and notably higher than that of pyrolitic melt under Earth's conditions (Bajgain et al., 2022; Caracas, 2024; Huang et al., 2024; Karki & Stixrude, 2010; Luo et al., 2021). This viscosity dependence on composition may behave similarly under higher pressures. Therefore, under more realistic scenarios involving multi-component magma oceans on super-Earths and sub-Neptunes, the viscosity may be even lower. The overall low viscosity of magma oceans of super-Earths and sub-Neptunes means large Rayleigh numbers, allowing for efficient flow and mixing. This could result in efficient differentiation and reduced lifetimes of airless magma oceans, although thickness atmospheres may exist and thus offset this effect.

4.3. Mass-Radius Relation of Hot Exoplanets

The mass-radius relation of a planet is primarily determined by its density profile, which depends on the equation of state of its constituent materials. Solid $MgSiO_3$ has long been considered a key endmember in the composition of exoplanets (Zeng et al., 2019). However, for hot exoplanets with molten mantles, assuming solid $MgSiO_3$ may introduce significant errors in predicting their radius for a given mass. The thermophysical properties of liquid $MgSiO_3$ provide essential constraints for accurately modeling the mass-radius relation of these planets.

We calculated the mass-radius relation for planets composed of liquid $MgSiO_3$. As shown in Figure 10, liquid $MgSiO_3$, being less dense than its solid counterpart, can notably increase the predicted radius of a planet for a given mass, although this effect diminishes with increasing planetary mass. The mass-radius relation for liquid $MgSiO_3$ helps refine the interpretation of planetary interiors, particularly for planets with high temperatures where solid-state assumptions fail. For example, the mass-radius data of the well-studied exoplanet 55 Cancri e aligns with that predicted by solid $MgSiO_3$ (Crida et al., 2018). Thus, its observed mass and radius cannot be explained by a solid $MgSiO_3$ mantle combined with a large Fe core, as Fe reduces the planetary radius for a given mass. Including liquid $MgSiO_3$ in the model allows for alternative interpretations of 55 Cancri e's composition, such as an Earth-like core-mantle structure with a partially molten mantle (likely different core mass fraction). This supports predictions that 55 Cancri e has extensive magma oceans. 55 Cancri e is also predicted to have a nitrogen/hydrogen-rich, carbon dioxide/monoxide-rich, or thin-metal-rich atmosphere (Hammond & Pierrehumbert, 2017; Hu et al., 2024; Ridden-Harper et al., 2016). In any case, future studies aiming to quantify 55 Cancri e's composition based on its mass-radius relation should rigorously take the difference between solid and liquid $MgSiO_3$ into account.

In recent years, more realistic and advanced planetary interior models have been proposed (Boujibar et al., 2020; Dorn et al., 2017; Dorn & Lichtenberg, 2021; Luo, Dorn, & Deng, 2024a; Luo, O'Rourke, & Deng, 2024b), which integrate the equations for mass conservation, hydrostatic equilibrium, thermal transport, and material-specific states into a unified framework. The properties of liquid silicate are critical parameters for these models. To better link observed mass-radius data with the composition, structure, and thermal states of exoplanets, future work should integrate liquid $MgSiO_3$ properties into advanced planetary models that account for the interplay between material properties, core-mantle boundary conditions, and compositional diversity. Additionally, the thermophysical properties of other liquid silicates at multi-megabar pressures require further quantification.

5. Conclusions

The liquid structure of $MgSiO_3$ evolves continuously with compression as manifested by decreasing bond lengths and increasing coordination numbers. The Si-O coordination number reached approximately 8 at 1,200 GPa. The O-O coordination number exhibits an interesting initial increase up to around 20–70 GPa, followed by a decrease, and then plateaus at about 300 GPa. The turnover at ~20–70 GPa correlates very well with the abundance of SiO_5 species. After the turnover, $MgSiO_3$ liquid displays solid-like behavior, including slow change in atomic

coordination numbers and a decrease in the Grüneisen parameter upon further compression. The complex behavior of the Grüneisen parameter with compression, including varying pressure and temperature dependence is well captured by the RTpress EOS. We further derive the adiabatic temperature profile and viscosity profile of magma oceans in super-Earths and sub-Neptunes. The findings indicate that the mantles of super-Earths and sub-Neptunes could solidify either starting from the bottom or at pressures near 120–150 GPa, depending on the mantle melting lines. The low viscosity of magma oceans likely enhances convective flows, leading to efficient differentiation. With these thermophysical properties quantified up to terapascal pressures, the mass-radius relationships of magma ocean exoplanets can be updated, revealing significant differences from their solid counterparts and underscoring the need to integrate these updates into future planetary interior models, particularly for hot exoplanets.

Data Availability Statement

Authors can confirm that all relevant data are included in the paper. Data used in the figures and examples of raw simulation outputs are available from Figshare (Luo, 2024). The Vienna Ab Initio Simulation Package (VASP) is a proprietary software available for purchase at https://www.vasp.at/. The RTpress EOS model is publicly available at https://github.com/aswolf/xmeos. The UMD package for performing liquid structure analysis is publicly available at https://github.com/rcaracas/UMD_package.

Acknowledgments
The work reported in this paper was conducted using the Princeton Research Computing, which is a consortium of groups led by the Princeton Institute for Computational Science and Engineering (PICSciE) and the Office of Information Technology's Research Computing. This material is based upon work supported by the National Science Foundation under Grant EAR- 2242946 to Jie Deng. We also acknowledge the support of the Dean for Research Innovation Funds for New Ideas in the Natural Sciences from Princeton University.

References

Angel, R., Gonzalez-Platas, J., & Alvaro, M. (2014). EosFit7c and a Fortran module (library) for equation of state calculations. *Zeitschrift für Kristallographie - Crystalline Materials*, *229*(5), 405–419. https://doi.org/10.1515/zkri-2013-1711

Bajgain, S., Ashley, A., Mookherjee, M., Ghosh, D., & Karki, B. (2022). Insights into magma ocean dynamics from the transport properties of basaltic melt. *Nature Communications*, *13*(1), 7590. Article 7590. https://doi.org/10.1038/s41467-022-35171-y

Bardon, L. (2018). *Silicate liquid in extreme conditions: Giant impacts and super-Earth interiors. Masters thesis (M. Phil)*. University College London.

Belonoshko, A. B., Skorodumova, N. V., Rosengren, A., Ahuja, R., Johansson, B., Burakovsky, L., & Preston, D. L. (2005). High-pressure melting of $MgSiO_3$. *Physical Review Letters*, *94*(19), 195701. Article 195701. https://doi.org/10.1103/PhysRevLett.94.195701

Blochl, P. E. (1994). Projector augmented wave method. *Physical Review B*, *50*(24), 17953–17979. https://doi.org/10.1103/PhysRevB.50.17953

Boehler, R., Ramakrishnan, J., & Kennedy, G. C. (1979). Grüneisen parameter of fluids and metals under compression. In K. D. Timmerhaus & M. S. Barber (Eds.), *High-Pressure Science and Technology*. Springer. https://doi.org/10.1007/978-1-4684-7470-1_150

Boujibar, A., Driscoll, P., & Fei, Y. (2020). Super-Earth internal structures and initial thermal states. *Journal of Geophysical Research-Planets*, *125*(5), e2019JE006124. Article e2019JE006124. https://doi.org/10.1029/2019je006124

Canup, R. (2004). Simulations of a late lunar-forming impact. *Icarus*, *168*(2), 433–456. https://doi.org/10.1016/j.icarus.2003.09.028

Caracas, R. (2024). The thermal equation of state of the magma Ocean. *Earth and Planetary Science Letters*, *637*, 118724. Article 118724. https://doi.org/10.1016/j.epsl.2024.118724

Caracas, R., Hirose, K., Nomura, R., & Ballmer, M. D. (2019). Melt-crystal density crossover in a deep magma ocean. *Earth and Planetary Science Letters*, *516*, 202–211. https://doi.org/10.1016/j.epsl.2019.03.031

Caracas, R., Kobsch, A., Solomatova, N., Li, Z., Soubiran, F., & Hernandez, J. (2021). Analyzing melts and fluids from Ab Initio molecular dynamics simulations with the UMD package. *Journal of Visualized Experiments*, *175*. https://doi.org/10.3791/61534

Caracas, R., & Stewart, S. (2023). No magma ocean surface after giant impacts between rocky planets. *Earth and Planetary Science Letters*, *608*, 118014. Article 118014. https://doi.org/10.1016/j.epsl.2023.118014

Charbonneau, D., Berta, Z. K., Irwin, J., Burke, C. J., Nutzman, P., Buchhave, L. A., et al. (2009). A super-Earth transiting a nearby low-mass star. *Nature*, *462*(7275), 891–894. https://doi.org/10.1038/nature08679

Crida, A., Ligi, R., Dorn, C., & Lebreton, Y. (2018). Mass, radius, and composition of the transiting planet 55 Cnc e: Using interferometry and correlations. *The Astrophysical Journal*, *860*(2), 122. https://doi.org/10.3847/1538-4357/aabfe4

de Koker, N., & Stixrude, L. (2009). Self-consistent thermodynamic description of silicate liquids, with application to shock melting of MgO periclase and $MgSiO_3$ perovskite. *Geophysical Journal International*, *178*(1), 162–179. https://doi.org/10.1111/j.1365-246X.2009.04142.x

Deng, J., Niu, H., Hu, J., Chen, M., & Stixrude, L. (2023). Melting of $MgSiO_3$ determined by machine learning potentials. *Physical Review B*, *107*(6), 064103. https://doi.org/10.1103/PhysRevB.107.064103

Deng, J., & Stixrude, L. (2021). Deep fractionation of Hf in a solidifying magma ocean and its implications for tungsten isotopic heterogeneities in the mantle. *Earth and Planetary Science Letters*, *562*, 116873. https://doi.org/10.1016/j.epsl.2021.116873

Dorn, C., & Lichtenberg, T. (2021). Hidden water in Magma Ocean exoplanets. *The Astrophysical Journal Letters*, *922*(1), L4. Article L4. https://doi.org/10.3847/2041-8213/ac33af

Dorn, C., Venturini, J., Khan, A., Heng, K., Alibert, Y., Helled, R., et al. (2017). A generalized Bayesian inference method for constraining the interiors of super Earths and sub-Neptunes. *Astronomy & Astrophysics*, *597*, A37. Article A37. https://doi.org/10.1051/0004-6361/201628708

Elkins-Tanton, L. (2012). Magma Oceans in the Inner solar system. *Annual Review of Earth and Planetary Sciences*, *40*(1), 113–139. https://doi.org/10.1146/annurev-earth-042711-105503

Fei, Y. W., Seagle, C. T., Townsend, J. P., McCoy, C. A., Boujibar, A., Driscoll, P., et al. (2021). Melting and density of $MgSiO_3$ determined by shock compression of bridgmanite to 1254GPa. *Nature Communications*, *12*(1), 876. Article 876. https://doi.org/10.1038/s41467-021-21170-y

Flyvbjerg, H., & Petersen, H. G. (1989). Error estimates on averages of correlated data. *Journal of Chemical Physics*, *91*(1), 461–466. https://doi.org/10.1063/1.457480

Fortney, J. J., Marley, M. S., & Barnes, J. W. (2007). Planetary radii across five orders of magnitude in mass and stellar insolation: Application to transits. *The Astrophysical Journal*, *659*(2), 1661–1672. https://doi.org/10.1086/512120

Fratanduono, D., Millot, M., Kraus, R., Spaulding, D., Collins, G., Celliers, P., & Eggert, J. (2018). Thermodynamic properties of $MgSiO_3$ at super-Earth mantle conditions. *Physical Review*, *97*(21), 214105. Article 214105. https://doi.org/10.1103/PhysRevB.97.214105

Fulton, B. J., Petigura, E. A., Howard, A. W., Isaacson, H., Marcy, G. W., Cargile, P. A., et al. (2017). The California-Kepler Survey. III. A gap in the radius distribution of small planets. *The Astronomical Journal*, *154*(3), 109. Article 109. https://doi.org/10.3847/1538-3881/aa80eb

González-Cataldo, F., Soubiran, F., Peterson, H., & Militzer, B. (2020). Path integral Monte Carlo and density functional molecular dynamics simulations of warm dense $MgSiO_3$. *Physical Review B*, *101*(2), 024107. Article 024107. https://doi.org/10.1103/PhysRevB.101.024107

Hammond, M., & Pierrehumbert, R. T. (2017). Linking the climate and thermal phase curve of 55 Cancri e. *The Astrophysical Journal*, *849*(2), 152. Article 152. https://doi.org/10.3847/1538-4357/aa9328

Hinkel, N. R., Youngblood, A., & Soares-Furtado, M. (2024). Host stars and how their compositions influence exoplanets. *Reviews in Mineralogy and Geochemistry*, *90*(1), 1–26. https://doi.org/10.2138/rmg.2024.90.01

Holland, T., & Powell, R. (1998). An internally consistent thermodynamic data set for phases of petrological interest. *Journal of Metamorphic Geology*, *16*(3), 309–343. https://doi.org/10.1111/j.1525-1314.1998.00140.x

Holmström, E., & Stixrude, L. (2015). Spin crossover in ferropericlase from first-principles molecular dynamics. *Physical Review Letters*, *114*(11), 117202. https://doi.org/10.1103/PhysRevLett.114.117202

Hu, R., Bello-Arufe, A., Zhang, M., Paragas, K., Zilinskas, M., van Buchem, C., et al. (2024). A secondary atmosphere on the rocky exoplanet 55 Cancri e. *Nature*, *630*(8017), 609–612. https://doi.org/10.1038/s41586-024-07432-x

Huang, D., Li, Y., & Murakami, M. (2024). Low viscosity of peridotite liquid: Implications for magma ocean dynamics. *Geophysical Research Letters*, *51*(7), e2023GL107608. Article e2023GL107608. https://doi.org/10.1029/2023GL107608

Karki, B. (2010). First-principles molecular dynamics simulations of silicate melts: Structural and dynamical properties. *Reviews in Mineralogy and Geochemistry*, *71*(1), 355–389. https://doi.org/10.2138/rmg.2010.71.17

Karki, B., & Stixrude, L. (2010). Viscosity of $MgSiO_3$ liquid at Earth's mantle conditions: Implications for an early magma ocean. *Sceince*, *328*(5979), 740–742. https://doi.org/10.1126/science.1188327

Kim, Y., Yi, Y., Kim, H., Chow, P., Xiao, Y., Shen, G., & Lee, S. (2019). Structural transitions in $MgSiO_3$ glasses and melts at the core-mantle boundary observed via inelastic X-ray scattering. *Geophysical Research Letters*, *46*(23), 13756–13764. https://doi.org/10.1029/2019GL085889

Kresse, G., & Furthmüller, J. (1996). Efficiency of ab-initio total energy calculations for metals and semiconductors using a plane-wave basis set. *Computational Materials Science*, *6*(1), 15–50. https://doi.org/10.1016/0927-0256(96)00008-0

Kresse, G., & Joubert, D. (1999). From ultrasoft pseudopotentials to the projector augmented-wave method. *Physical Review B*, *59*(3), 1758–1775. https://doi.org/10.1103/PhysRevB.59.1758

Luo, H. (2024). Structure, thermodynamics, and viscosity of MgSiO3 liquid in super-Earths and sub-Neptunes [Dataset]. *Figshare*. https://doi.org/10.6084/m9.figshare.26543653.v1

Luo, H., Dorn, C., & Deng, J. (2024). The interior as the dominant water reservoir in super-Earths and sub-Neptunes. *Nature Astronomy*, *8*(11), 1399–1407. https://doi.org/10.1038/s41550-024-02347-z

Luo, H., O'Rourke, J., & Deng, J. (2024). Radiogenic heating sustains long-lived volcanism and magnetic dynamos in super-Earths. *Science Advances*, *10*(37). https://doi.org/10.1126/sciadv.ado7603

Luo, H. Y., Karki, B. B., Ghosh, D. B., & Bao, H. M. (2021). Anomalous behavior of viscosity and electrical conductivity of $MgSiO_3$ melt at mantle conditions. *Geophysical Research Letters*, *48*(13), e2021GL093573. Article e2021GL093573. https://doi.org/10.1029/2021gl093573

Mermin, N. D. (1965). Thermal properties of the inhomogeneous electron gas. *Physical Review*, *137*(5A), A1441–A1443. https://doi.org/10.1103/PhysRev.137.A1441

Militzer, B. (2013). Ab initio investigation of a possible liquid liquid phase transition in $MgSiO_3$ at megabar pressures. *High Energy Density Physics*, *9*(1), 152–157. https://doi.org/10.1016/j.hedp.2012.11.006

Morard, G., Hernandez, J., Pege, C., Nagy, C., Libon, L., Lacquement, A., et al. (2024). Structural evolution of liquid silicates under conditions in Super-Earth interiors. *Nature Communications*, *15*(1), 8483. Article 8483. https://doi.org/10.1038/s41467-024-51796-7

Mosenfelder, J. L., Asimow, P. D., Frost, D. J., Rubie, D. C., & Ahrens, T. J. (2009). The $MgSiO_3$ system at high pressure: Thermodynamic properties of perovskite, postperovskite, and melt from global inversion of shock and static compression data. *Journal of Geophysical Research*, *114*(B1), B01203. https://doi.org/10.1029/2008JB005900

Nose, S. (1984). A unified formulation of the constant temperature molecular dynamics methods. *Journal of Chemical Physics*, *81*(1), 511–519. https://doi.org/10.1063/1.447334

Perdew, J. P., Ruzsinszky, A., Csonka, G. I., Vydrov, O. A., Scuseria, G. E., Constantin, L. A., et al. (2008). Restoring the density-gradient expansion for exchange in solids and surfaces. *Physical Review Letters*, *100*(13), 136406. Article 136406. https://doi.org/10.1103/PhysRevLett.100.136406

Ridden-Harper, A. R., Snellen, I. A. G., Keller, C. U., De Kok, R. J., Di Gloria, E., Hoeijmakers, H. J., et al. (2016). Search for an exosphere in sodium and calcium in the transmission spectrum of exoplanet 55 Cancri e. *Astronomy & Astrophysics*, *593*, A129. Article A129. https://doi.org/10.1051/0004-6361/201628448

Root, S., Townsend, J., Davies, E., Lemke, R., Bliss, D., Fratanduono, D., et al. (2018). The principal Hugoniot of Forsterite to 950 GPa. *Geophysical Research Letters*, *45*(9), 3865–3872. https://doi.org/10.1029/2017GL076931

Scipioni, R., Stixrude, L., & Desjarlais, M. P. (2017). Electrical conductivity of SiO_2 at extreme conditions and planetary dynamos. *Proceedings of the National Academy of Sciences*, *114*(34), 9009–9013. https://doi.org/10.1073/pnas.1704762114

Solomatov, V. (2007). 9.04—Magma oceans and primordial mantle differentiation. In S. Gerald (Ed.), *Treatise on Geophysics* (pp. 91–119). Elsevier. https://doi.org/10.1016/B978-044452748-6.00141-3

Solomatova, N., & Caracas, R. (2019). Pressure-induced coordination changes in a pyrolitic silicate melt from Ab Initio molecular dynamics simulations. *Journal of Geophysical Research: Solid Earth*, *124*(11), 11232–11250. https://doi.org/10.1029/2019JB018238

Soubiran, F., & Militzer, B. (2018). Electrical conductivity and magnetic dynamos in magma oceans of Super-Earths. *Nature Communications*, *9*(1), 3883. Article 3883. https://doi.org/10.1038/s41467-018-06432-6

Spera, F., Ghiorso, M., & Nevins, D. (2011). Structure, thermodynamic and transport properties of liquid $MgSiO_3$: Comparison of molecular models and laboratory results. *Geochimica et Cosmochimica Acta*, *75*(5), 1272–1296. https://doi.org/10.1016/j.gca.2010.12.004

Stixrude, L. (2014). Melting in super-Earths. *Philosophical Transactions of the Royal Society A: Mathematical, Physical & Engineering Sciences*, *372*(2014), 20130076. Article 20130076. https://doi.org/10.1098/rsta.2013.0076

Stixrude, L., de Koker, N., Sun, N., Mookherjee, M., & Karki, B. (2009). Thermodynamics of silicate liquids in the deep Earth. *Earth and Planetary Science Letters*, *278*(3–4), 226–232. https://doi.org/10.1016/j.epsl.2008.12.006

Stixrude, L., & Karki, B. (2005). Structure and freezing of $MgSiO_3$ liquid in Earth's lower mantle. *Science*, *310*(5746), 297–299. https://doi.org/10.1126/science.1116952

Valencia, D., Sasselov, D. D., & O'Connell, R. J. (2007). Radius and structure models of the first Super-Earth planet. *The Astrophysical Journal*, *656*(1), 545–551. https://doi.org/10.1086/509800

Vazan, A., Ormel, C. W., Noack, L., & Dominik, C. (2018). Contribution of the core to the thermal evolution of sub-Neptunes. *The Astrophysical Journal*, *869*(2), 163. https://doi.org/10.3847/1538-4357/aaef33

Wolf, A., & Bower, D. (2018). An equation of state for high pressure-temperature liquids (RTpress) with application to $MgSiO_3$ melt. *Physics of the Earth and Planetary Interiors*, *278*, 59–74. https://doi.org/10.1016/j.pepi.2018.02.004

Zeng, L., Jacobsen, S. B., Sasselov, D. D., Petaev, M. I., Vanderburg, A., Lopez-Morales, M., et al. (2019). Growth model interpretation of planet size distribution. *Proceedings of the National Academy of Sciences of the United States of America*, *116*(20), 9723–9728. https://doi.org/10.1073/pnas.1812905116

Zhao, G., Mu, H., Tan, X., Wang, D., & Yang, C. (2014). Structural and dynamical properties of $MgSiO_3$ melt over the pressure range 200–500 GPa: Ab initio molecular dynamics. *Journal of Non-Crystalline Solids*, *385*, 169–174. https://doi.org/10.1016/j.jnoncrysol.2013.11.024